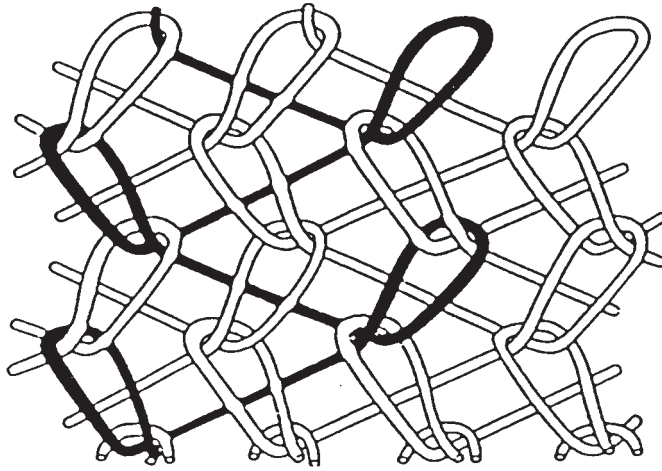

H. HAMADA, S. RAMAKRISHNA AND
Z.M. HUANG

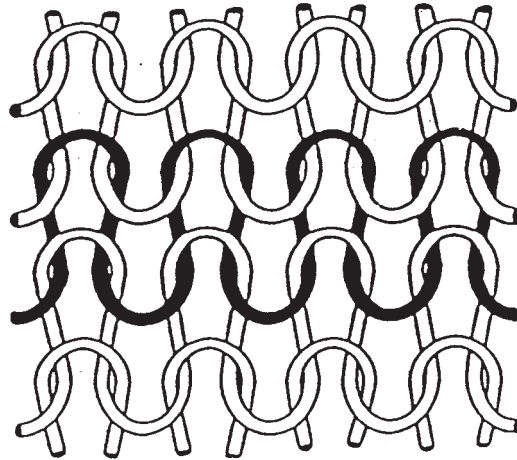
6.1 Introduction

In recent years, knitted fabric reinforcements have received great attention in the composites industry [1–10]. This is attributed to the unique properties of knitted fabrics compared with other reinforcement fabric structures such as woven and braid. Interlocking of loops of yarn makes knitted fabrics as shown in Fig. 6.1. Here, the term ‘yarns’ represents individual filaments, untwisted fiber bundles, twisted fiber bundles or roving. These loops can glide over each other and thus give a high degree of deformability to knitted fabrics. This deformability provides drapeability, which makes knitted fabric reinforcement formable into the desired complex preform shapes for liquid molding to produce the composite component. Moreover, the use of advanced knitting machines allows the production of near net shape fabrics such as domes, cones, T-pipe junctions, flanged pipes and sandwich fabrics. The use of near net shape preforms has the advantage of minimum material wastage. A combination of net shape fiber preforms and conventional liquid molding techniques has the potential to mass produce and to reduce the production time, and thus lower the cost of composite material. This is important especially when the applications for composite materials are changing from high-cost and high-performance products of aerospace industry to low-cost and mass-producible products of the general engineering industry.

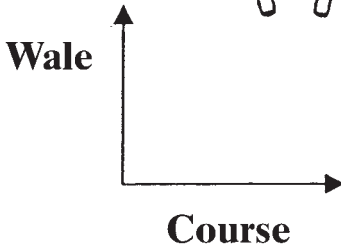
Knitted fabrics are basically categorized into two types, namely warp knit fabrics and weft knit fabrics, based on the knitting direction. Schematic diagrams of both the knitted fabrics are shown in Fig. 6.1. Warp knitted fabric is produced by knitting in the lengthwise direction (wale direction) of the fabric, as shown by a solid line in Fig. 6.1(a). Weft knitted fabric is produced by knitting in the widthwise direction (course direction) of the fabric (solid line in Fig. 6.1b). Several types of knitted fabrics are used in the garment industry for fashion purposes [11]. However, only a limited number of knit structures are being investigated for composites in engineering applications,



(a)



(b)



6.1 Schematic diagrams of (a) warp knitted and (b) weft knitted fabrics.

Copyrighted Material downloaded from Woodhead Publishing Online
Delivered by http://woodhead.metapress.com
Hong Kong Polytechnic University (714-57-975)
Saturday, January 22, 2011 12:30:57 AM
IP Address: 158.132.122.9

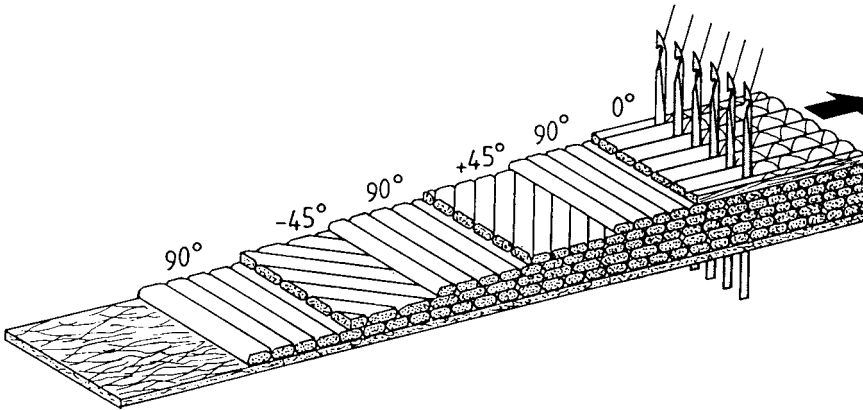
Table 6.1. Classification of typical warp and weft knitted fabrics used in engineering applications

Type	Fabric classification	Weft knitted fabric structure	Warp knitted fabric structure
I	2-D fabric	Plain, rib, Milano rib, inlaid fabrics	Dembigh, Atlas
II	2-D fabric – 3-D shape	Plain, rib	Dembigh, Atlas
III	3-D solid fabric	Plain and rib fabrics with inlay fiber yarns	Multiaxial warp knitted fabrics or noncrimp fabrics
IV	3-D hollow fabric (sandwich fabric)	Single jersey face structure	Single Dembigh face structure

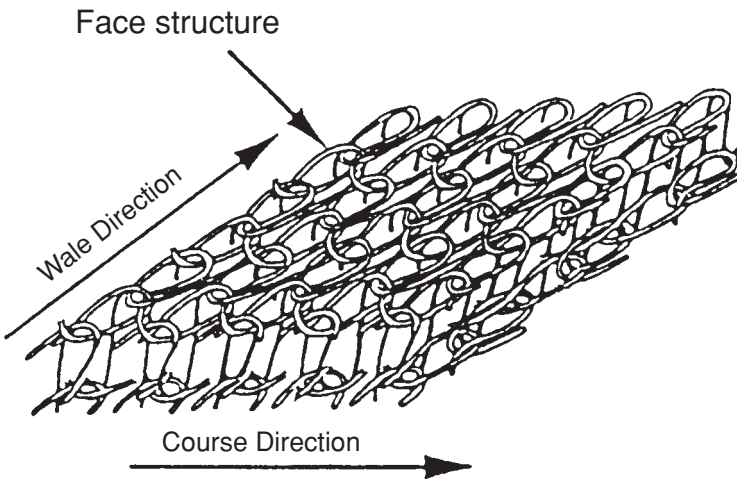
since: (a) most engineering applications require only simple knit structures and (b) unlike textile fibers (cotton and polyester), it is difficult to form stiff reinforcement fibers such as glass, carbon and aramid into complicated knit structures. Typical warp and weft knitted fabrics investigated for engineering applications are summarized in Table 6.1.

Both the warp and weft knitted fabrics can be further classified into four types based on the dimensional (D) arrangement of yarns. Type I fabrics are simple 2-D flat knitted fabrics shown in Fig. 6.1. These fabrics can be cut to the required dimensions and laminated just as in conventional woven fabric composites. Using fully fashioned knitting machines it is possible to produce 2-D fabrics into the net shape of the components. Such 2-D fabrics with 3-D shapes may be categorized as Type II fabrics. As mentioned above, the combination of Type II fabrics with conventional composite molding techniques, makes it possible to cut down the fabrication costs. Type III fabrics are produced by stitching multiaxial layers of parallel yarn [12]. Because of minimum fiber crimp, they are also called non-crimp fabrics. A schematic diagram of a typical Type III fabric is shown in Fig. 6.2. Owing to their superior properties and better drapeability than the woven fabric composites, they are being considered for building buses, trucks, ships and aircraft wings. Type IV fabrics, also known as sandwich fabrics or 3-D hollow fabrics, are produced by binding 2-D-face fabrics together using pile yarns [13]. A schematic diagram of a typical Type IV fabric is shown in Fig. 6.3. These fabrics are sometimes referred to as 2.5-D fabrics, as the amount of fibers in the thickness direction is less than the fibers in the planar direction of the fabric. They are considered to achieve the optimum design of high-performance and damage-tolerant composite structures.

The objective of this chapter is to model the mechanical behavior of



6.2 Schematic representation of a multiaxial warp knitted fabric.



6.3 Schematic diagram of a warp knitted sandwich fabric.

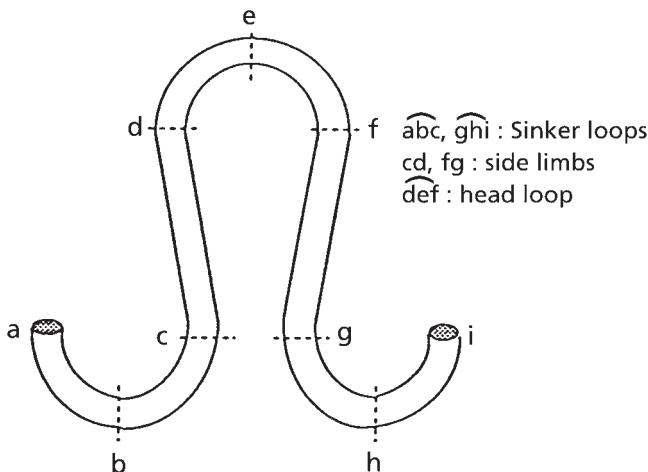
Type I knitted fabric reinforced composites. However, the procedures described here can be easily generalized to the composites reinforced with other kinds of knitted fabrics. The presentations of this chapter begin with a geometric description of Type I plain weft knitted fabric, followed by a description of the tensile behavior of knitted fabric reinforced composites obtained from experimental studies. Analytical procedures for modeling the elastic and strength properties of knitted fabric composites are then presented. The analytical modeling work reported in this chapter is based upon references [11,14–21].

6.2 Description of knitted fabric

Let us consider the plain weft knitted fabric shown in Fig. 6.1(b). The knit structure is formed by interlooping of one yarn system into continuously connecting vertical columns and horizontal rows of loops. This type of fabric can be produced using either flat bed or circular knitting machines. The vertical column of loops along the length of the fabric is called 'wale' and the horizontal row of loops along the width of the fabric is called 'course'. The respective directions are called 'wale direction' and 'course direction'. A single knit loop comprises a head loop, two side limbs and two sinker loops as shown in Fig. 6.4. Changing the structure of knit loops produces different knitted fabrics. Knitted fabrics are often specified using 'wale density' and 'course density'. The wale density (W) is defined as the number of wales per unit length in the course direction. Similarly, the course density (C) is the number of courses per unit length in the wale direction of the fabric. Both the wale and course densities are mainly determined by the gauge of the knitting machine, i.e. the number of needles per unit length of the machine bed. The product of C and W gives the stitch density, N , of the fabric. N is defined as the number of knit loops per unit planar area of the fabric.

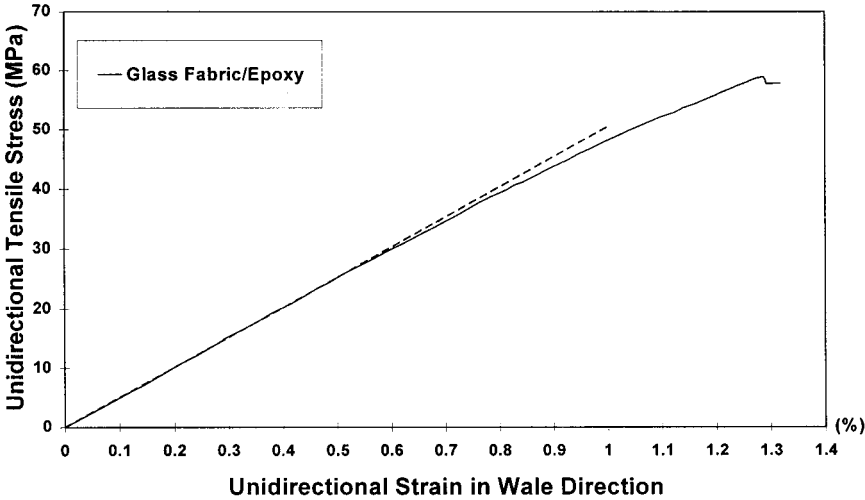
6.3 Tensile behavior of knitted fabric composites

Composites are fabricated by impregnating knitted fabric of reinforcement fiber yarns with the matrix polymer. For a given knitted fabric structure, the mechanical behavior of composite material depends on the properties of

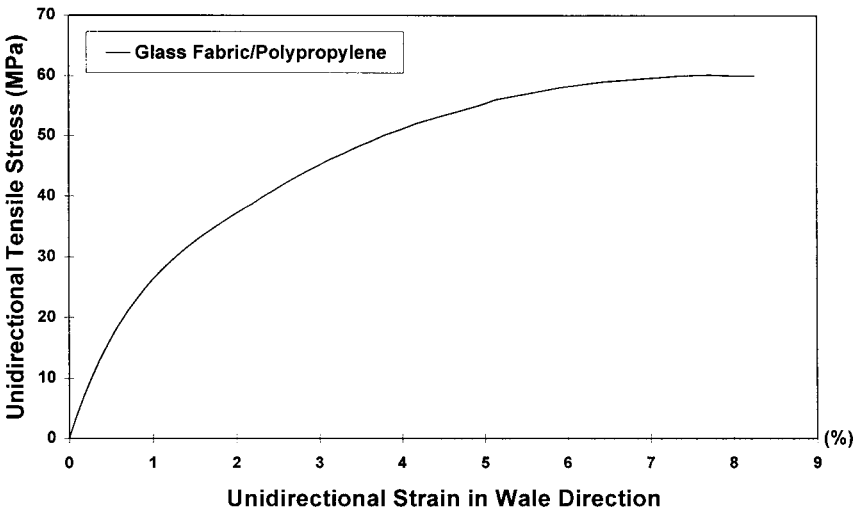


6.4 Schematic representation of various portions of a typical knit loop.

the constituent fiber and matrix materials [22–26]. Typical tensile stress–strain curves of three different kinds of knitted fabric composites are shown in Fig. 6.5. These curves are obtained from tensile testing in the wale direction of the composite. The tensile stress–strain curve of composite made from knitted glass fiber fabric and epoxy matrix is grossly linear with

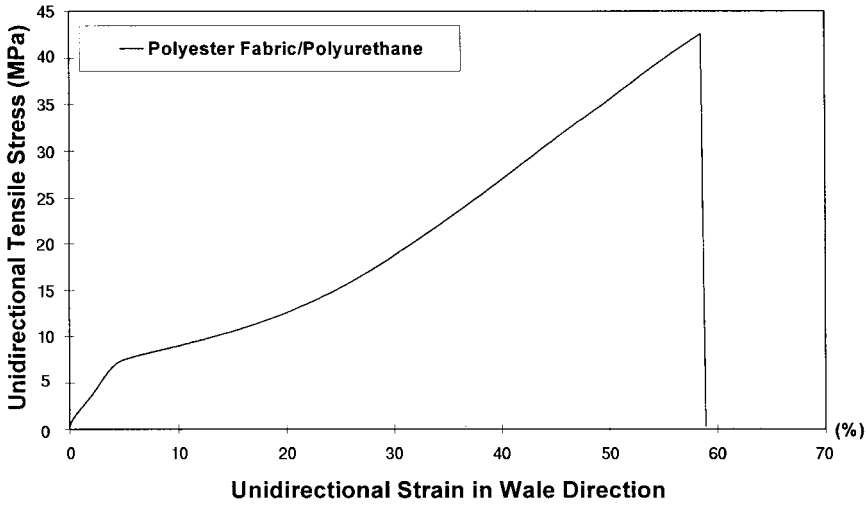


(a)



(b)

6.5 Typical tensile stress–strain curves of (a) knitted glass fiber fabric reinforced epoxy composite, (b) knitted glass fiber fabric reinforced polypropylene composite, and (c) knitted polyester fiber fabric reinforced polyurethane composite.

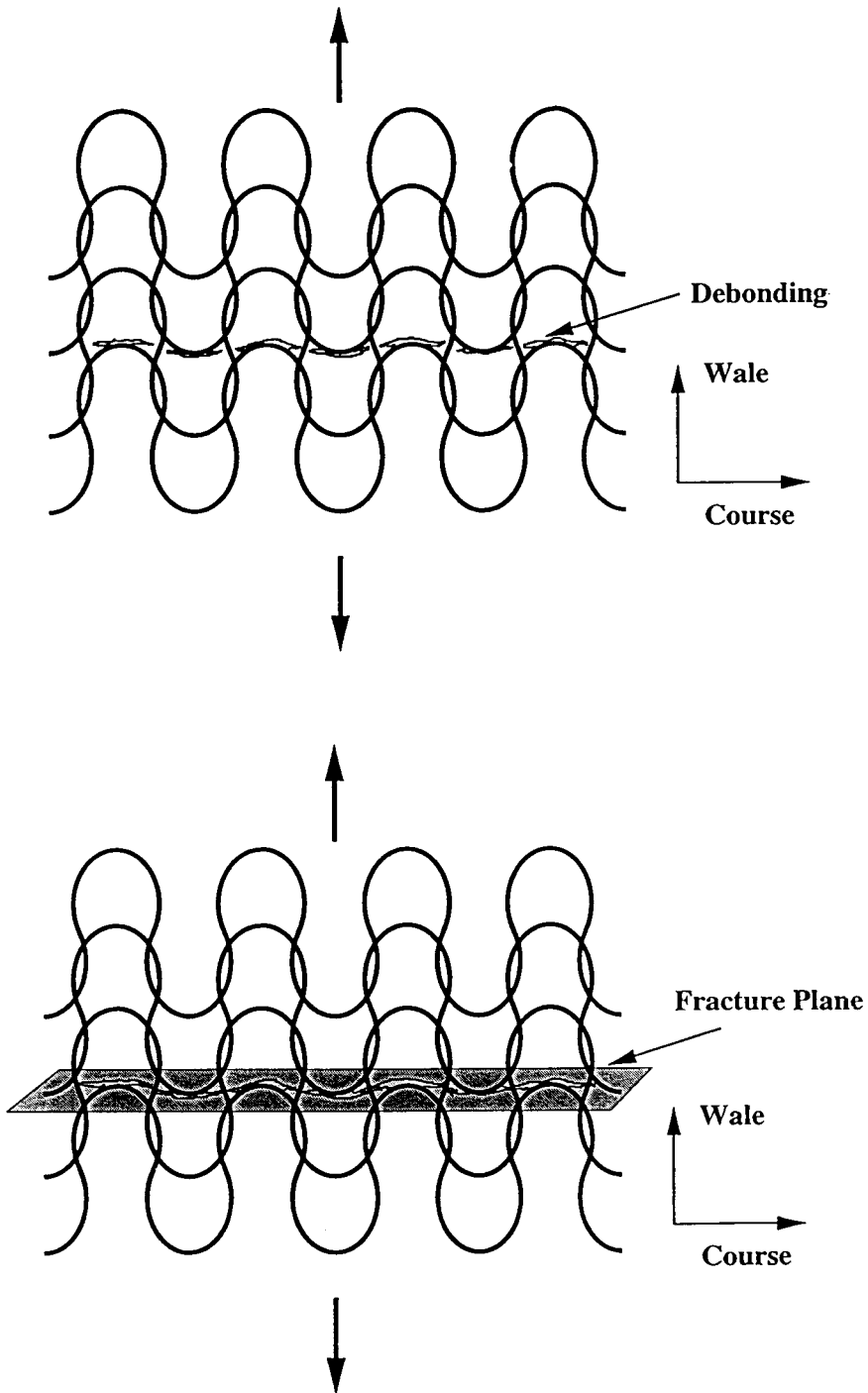


(c)

6.5 (cont.)

a small ultimate failure strain, 1.3%. In the case of knitted glass fiber fabric reinforced polypropylene composite material, the stress-strain curve changes from an initial linearly elastic relationship to a significantly non-linear relationship with an intermediate ultimate failure strain of 8.5%. The matrix polymer used in these composite materials mainly causes this difference. At the other end of the spectrum, a highly flexible stress-strain behavior could be achieved by reinforcing elastomeric material with a knitted fabric. A typical stress-strain curve of a knitted polyester fiber fabric reinforced polyurethane elastomer is shown in Fig. 6.5. The stress-strain behavior is characterized by a small initial linear elastic relationship, followed by nonlinear behavior with large ultimate failure strain of 60%. In other words, by selecting the type of matrix and reinforcement materials, the mechanical characteristics of a knitted fabric composite can be tailored from rigid to flexible.

This chapter mainly concerns the mechanical behavior of the knitted glass fiber fabric reinforced epoxy composites, in which the stresses and strains are connected by fixed linear relationships. Hence, let us consider the tensile behavior of knitted glass fiber fabric reinforced epoxy composite in detail. The stress-strain curve is linear up to the knee point, which occurred at approximately 0.45% strain. Above the knee point, the material deformation and microfracture processes in the specimen cause the non-linearity. A schematic representation of a typical fracture process in a knitted fabric composite is given in Fig. 6.6. At strain levels immediately



6.6 Schematic representation of a typical fracture process in tensile tested knitted fabric composite.

above the knee point, debonding of yarns oriented normal to the testing direction occurs. The cracks nucleated from the debonded sites propagate into resin-rich regions and coalesce into large transverse cracks. Unfractured yarns bridge the fracture plane. The ultimate fracture of the tensile specimen occurs upon the fracture of bridging yarns. In other words, the tensile strength of composite material is determined mainly by the fracture strength of yarns bridging the fracture plane.

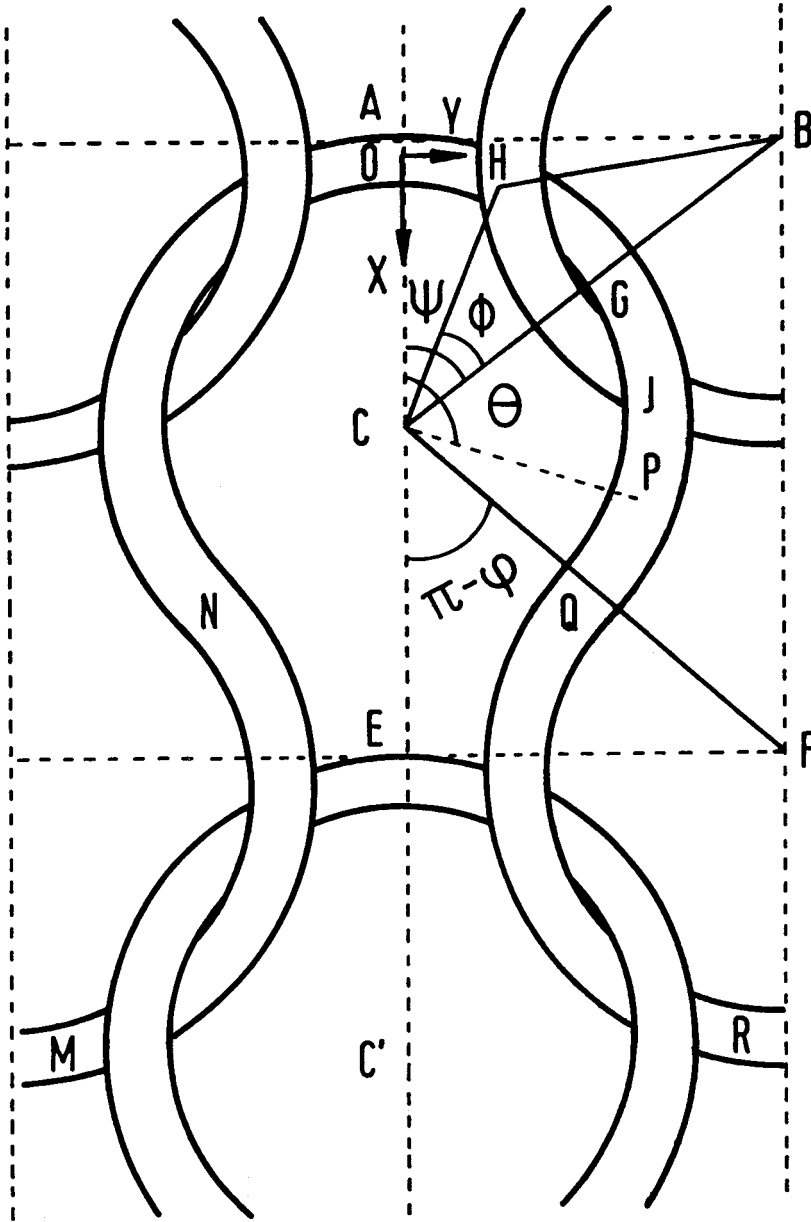
6.4 Analysis of 3-D elastic properties

6.4.1 Methodology of analysis

The plain weft knitted fabric reinforced composite material investigated in this study is assumed to have only reinforcement fiber yarns and polymer matrix. For analysis purposes, a unit cell representing the complete knitted fabric composite is identified. A geometric model is proposed to determine the orientation of yarn in the composite (Section 6.4.2). Section 6.4.3 outlines the procedure for estimating the fiber volume fraction of the composite. The unit cell is divided into four representative volumes, also called a 'crossover model'. The crossover model is further divided into sub-volumes, which are considered as transversely isotropic unidirectional fiber reinforced composites. A new micromechanical model is used to predict all the five independent elastic constants of the unidirectional fiber reinforced composites (Section 6.4.4). By considering the contributions of both the fibers and net matrix material, the compliance/stiffness matrix of each sub-volume in the material co-ordinate system is calculated using the new formulae. This compliance/stiffness matrix of each sub-volume is then transformed to the global co-ordinate system (see Section 6.4.5). A volume-averaging scheme has been applied to obtain the overall compliance/stiffness matrix of the knitted fabric composite (Section 6.4.6). The effects of fiber content and other parameters of knitted fabric on the elastic properties of the composite material are identified (Section 6.4.7).

6.4.2 Geometric model

A schematic diagram of an idealized unit cell of the plain weft knitted fabric is given in Fig. 6.7. The basic assumption is that the projection of the central axis of the yarn loop on the fabric plane is composed of circular arcs. This assumption is reasonable as the knit loops are formed during knitting by bending the yarns round a series of equally spaced knitting needles and sinkers. The physical meanings of various symbols used below are also shown in the figure. The geometry of the unit cell can be described using



6.7 Schematic diagram of an idealized unit cell of the plain weft knitted fabric.

Copyrighted Material downloaded from Woodhead Publishing Online
 Delivered by http://woodhead.metapress.com
 Hong Kong Polytechnic University (714-57-975)
 Saturday, January 22, 2011 12:30:57 AM
 IP Address: 158.132.122.9

three parameters, i.e. wale density, W , course density, C , and the yarn diameter, d .

In the fabric plane, we set the global rectangular axis Ox to be parallel to the wale direction and Oy to the course direction. Suppose that the OQ portion of the loop has a center at C with a total angle φ , i.e. $OCQ = \varphi$. ' ad ' denotes the radius of projection of the loop, i.e. the length between O and C , where a is a constant. Q is the point at which the central axis of this loop joins the central axis of the loop with a center F . H and J are the points at which the yarns of adjacent loops (loops with centers at C and B) cross over. The angles $OCB = \psi$ and $HCB = \phi$. Let P be any point on the central axis of the loop and the angle of the projection of the loop portion from O to P be θ , $OCP = \theta$. The co-ordinates of P are given by

$$\begin{aligned}x &= ad(1 - \cos \theta) \\y &= ad \sin \theta \\z &= \frac{hd}{2} \left[1 - \cos \left(\pi \frac{\theta}{\varphi} \right) \right]\end{aligned} \quad [6.1]$$

where h is a constant used for representing maximum height hd (at Q) of the central axis above the plane of the fabric. The parameters a , h and φ in (6.1) are determined from the following formulae:

$$a = \frac{1}{4Wd \sin \varphi} \quad [6.2]$$

$$\varphi = \pi + \sin^{-1} \left(\frac{C^2 d}{[C^2 + W^2(1 - C^2 d^2)]^{1/2}} \right) - \tan^{-1} \left[\frac{C}{W(1 - C^2 d^2)} \right] \quad [6.3]$$

$$h = \left[\sin \left(\pi \frac{\psi}{\varphi} \right) \sin \left(\pi \frac{\phi}{\varphi} \right) \right]^{-1} \quad [6.4]$$

$$\psi = \sin^{-1} \left(\frac{2a}{2a-1} \sin \varphi \right) \quad [6.5]$$

$$\phi = \cos^{-1} \left(\frac{2a-1}{2a} \right) \quad [6.6]$$

The yarn diameter d can be expressed in terms of the linear density (D_y) of the yarn and packing fraction (K) of fibers in the yarn as

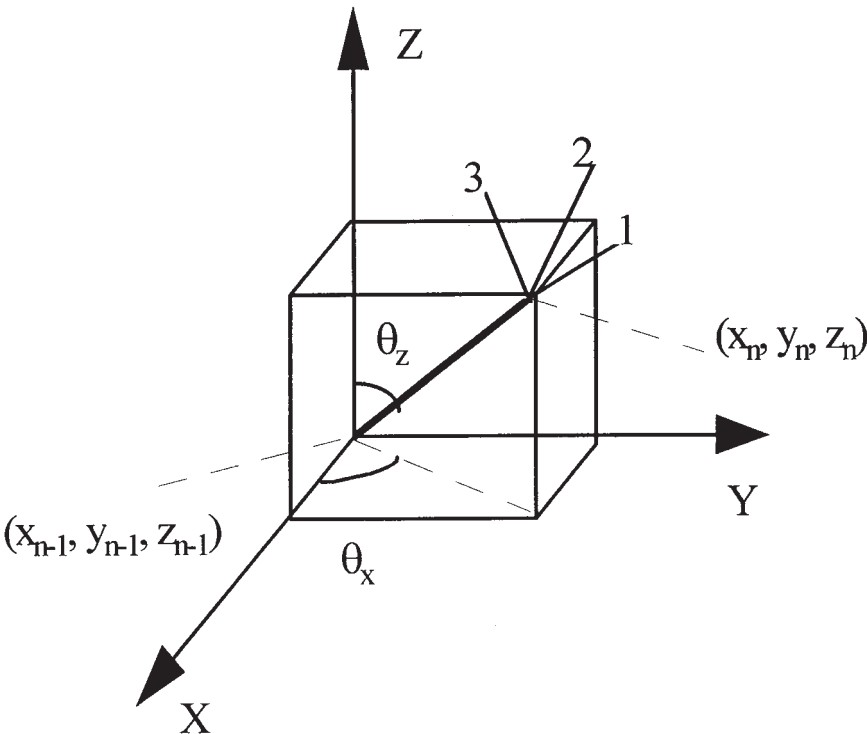
$$d = \frac{2}{3} \sqrt{\frac{D_y}{10\pi\rho_f K}} \times 10^{-2} \text{ (cm)} \quad [6.7]$$

where ρ_f is the density of fiber (g/cm^3).

From Fig. 6.7, it is clear that the orientation of the yarn in a knit loop (MNOQP) can be determined from knowing the orientation of the yarn in the portion OQ. We may assume that the OQ portion is an assemblage of a series of straight segments. Let $(x_{n-1}, y_{n-1}, z_{n-1})$ and (x_n, y_n, z_n) be the coordinates of start and end points of the $(n - 1)$ th yarn segment (see Fig. 6.8). The orientation of the segment in 3-D co-ordinates can be specified using two angles, θ_x and θ_z , where θ_z is the angle between the z -axis and the yarn segment and θ_x the angle between the x -axis and the projected straight line of the segment on the x - y plane. These two angles are important in our geometric analysis. They are determined as

$$\theta_x = \operatorname{tg}^{-1} \left(\frac{y_n - y_{n-1}}{x_n - x_{n-1}} \right) \quad [6.8]$$

$$\theta_z = \operatorname{tg}^{-1} \left[\frac{\sqrt{(x_n - x_{n-1})^2 + (y_n - y_{n-1})^2}}{z_n - z_{n-1}} \right] \quad [6.9]$$



6.8 Representation of a segment of yarn.

Equations 6.8 and 6.9 imply that only relative co-ordinates of the yarn are important. Therefore, we can replace the unit cell shown in Fig. 6.7 with the unit cell in Fig. 6.9(a). The unit cell in Fig. 6.9(a) can be further divided into four identical sub-cells. Each sub-cell consists of two impregnated yarns which cross over each other. This sub-cell is known as the crossover model [16] and is represented in Fig. 6.9(b). Using the crossover model, a unit cell can be constructed. Repeating the unit cell in the fabric plane will obviously reproduce the complete plain knitted fabric structure. We thus only need to investigate the crossover model which is taken as a representative volume. The co-ordinates of the first yarn in the model are given by Equation 6.1 with $0 \leq \theta \leq \varphi$. To determine the co-ordinates of the second yarn easily, we choose its starting point to be nearer to the end point of the first yarn. The co-ordinates of the points on the second yarn are thus given by

$$x_1^{2\text{nd}} = 2ad - \frac{1}{2Wt\text{g}(\psi)}$$

$$y_1^{2\text{nd}} = \frac{1}{2W}$$

$$z_1^{2\text{nd}} = z_1^{1\text{st}}$$

$$x_n^{2\text{nd}} = x_1^{2\text{nd}} - x_n^{1\text{st}}$$

$$y_n^{2\text{nd}} = y_1^{2\text{nd}} - y_n^{1\text{st}}$$

$$z_n^{2\text{nd}} = z_n^{1\text{st}} \quad n \geq 2, 3, \dots$$

6.4.3 Estimation of fiber volume fraction

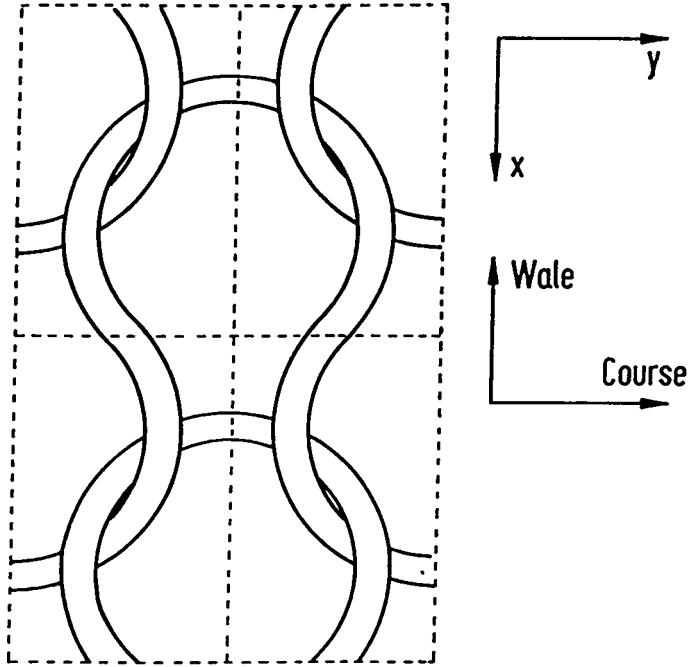
Based on the above-mentioned geometric model, the fiber volume fraction of the knitted fabric composite is given by [11]:

$$V_f = \frac{n_k D_y L_s C W}{9\rho_f A t} \times 10^{-5} \quad [6.10]$$

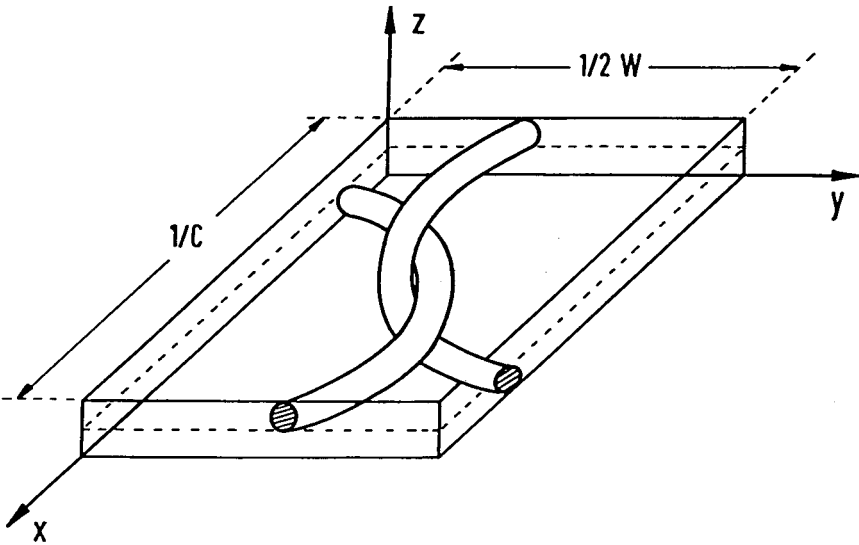
where n_k is the number of plies of the fabric in the composite, t is the thickness of the composite measured in centimeters, A is the planar area over which W and C are measured, and L_s is the length of yarn in one loop of the unit cell which can be represented approximately by

$$L_s \approx 4(ad)\varphi \quad [6.11]$$

Let us apply Equation 6.10 to the knitted glass fiber fabric reinforced epoxy composites described in Section 6.3. Knitted fabrics with $W = 2$ loops/cm and $C = 2.5$ loops/cm, are made using 1600 denier (D_y) glass fiber yarns (fiber density $\rho_f = 2.54 \text{ g/cm}^3$). Composites with single and four plies of



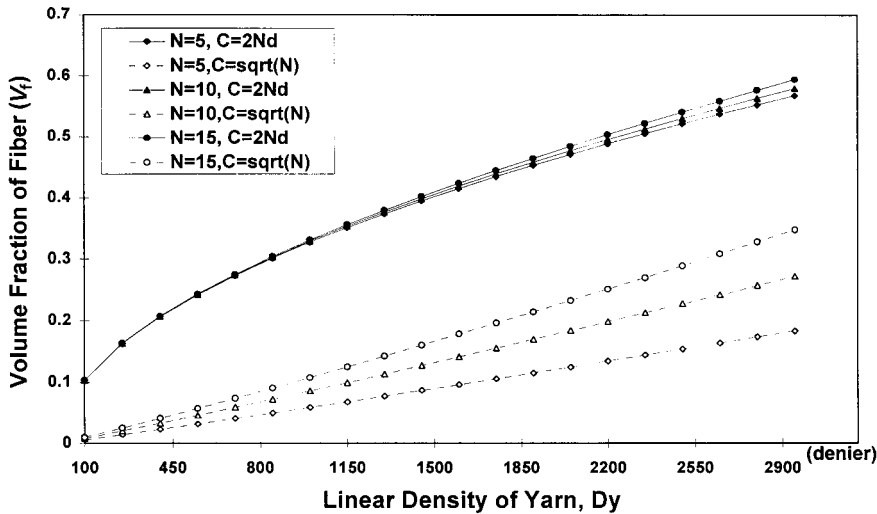
(a)



(b)

6.9 Schematic diagrams of (a) unit cell and (b) crossover model.

Copyrighted Material downloaded from Woodhead Publishing Online
 Delivered by http://woodhead.metapress.com
 Hong Kong Polytechnic University (714-57-975)
 Saturday, January 22, 2011 12:30:57 AM
 IP Address: 158.132.122.9

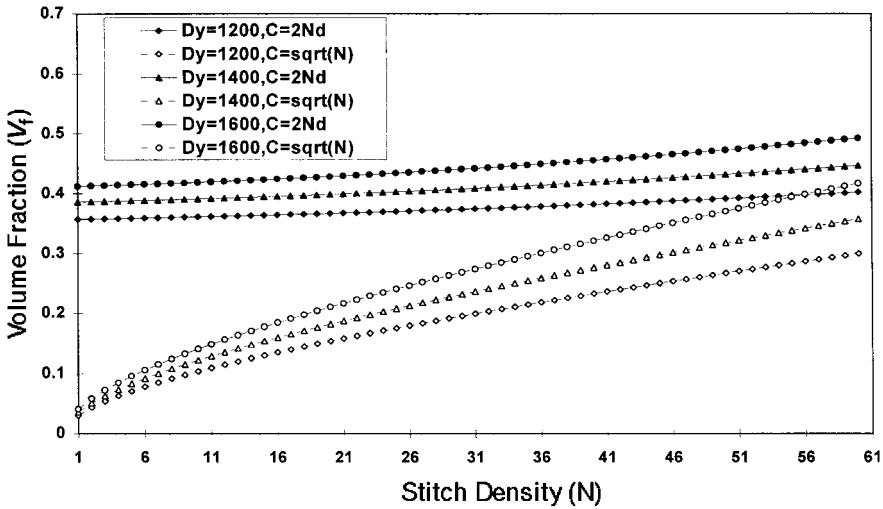


6.10 Typical variation of volume fraction of fibers with the linear density of yarn.

knitted fabric contained 0.095 and 0.323, respectively, volume fraction of fibers. These fiber volume fractions are determined experimentally by the combustion method. The single-ply and four-ply composites have $t = 0.06$ and 0.07 cm, respectively. More details on the fabrication and testing of plain weft knitted glass fiber fabric reinforced epoxy composites can be found elsewhere [22,23]. Using Equation 6.10 the estimated fiber volume fractions are 0.0933 and 0.3198 for single- and four-ply composites, respectively. The predicted fiber volume fractions are found to be close to those determined from the experiments. Therefore, this equation will be used to study the variation of fiber volume fraction with the changes in the parameters of knitted fabric.

By assuming that it is possible to use yarns of different sizes, the variation of V_f with D_y is computed theoretically. Figure 6.10 gives an estimate of V_f that can be expected when different sizes of yarn are used. For a given stitch density of knitted fabric ($N = C \times W$), the V_f increased linearly with increasing D_y . In other words, the fiber content of knitted fabric composites can be increased with increasing D_y . However, the maximum V_f that can be achieved is limited by the knitting needles used in the knitting machine. Increasing D_y means coarser yarns. In general, the coarser yarns are difficult to knit and the coarsest yarn that can be used is dependent on the yarn type, knitting needle size and other devices used on the knitting machine.

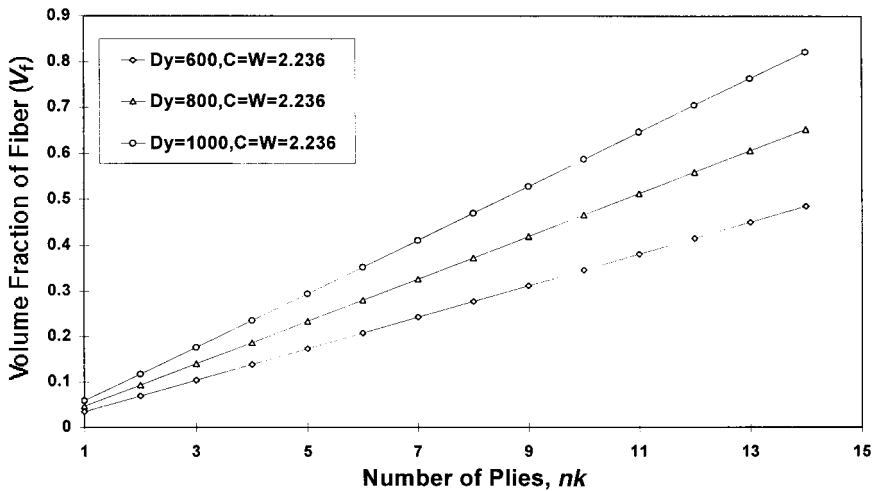
For a constant D_y , the variation of V_f with N is shown in Fig. 6.11. The N



6.11 Typical variation of volume fraction of fibers with the stitch density of knitted fabric.

of knitted fabric can be changed in two ways: (1) machine gauge and (2) stitch tightness control setting on the knitting machine. Machine gauge is defined as the number of needles per unit length of needle bed in the knitting machine. Most machines are equipped with a stitch tightness control button, so that it is possible to alter N in a range. Figure 6.11 suggests that V_f increases non-linearly with increasing N . This can be understood by examining Equation 6.10. D_y and other parameters in the denominator of Equation 6.10 are assumed to be constant. Hence, V_f is proportional to the product of L_s and N . An increase of N means smaller knit loops which implies that stitch length, L_s , decreases with increasing N . The inverse relationship between the N and L_s results in non-linear variation of V_f with increasing N . Nevertheless, it can be said that V_f can be increased with increasing N . The maximum V_f that can be achieved with increasing N is limited by the yarn diameter, d . With increasing stitch density the course spacing, $1/C$, and wale spacing, $1/W$, decrease. In other words, the side limbs of knit loop come closer with increasing stitch density or tightness of knitted fabric. The spacing between the limbs of a loop is approximately $\frac{1}{2}W$. The minimum spacing of side limbs is limited by the yarn diameter. To be able to stitch a knitted fabric, the condition ($\frac{1}{2}W \geq d$) needs to be satisfied. The plots in Fig. 6.12 give an approximate idea of the different V_f that can be achieved by changing N .

The relation between V_f and number of plies of knitted fabric (n_k) is shown in Fig. 6.12. For given D_y and N , the V_f can be increased with increas-



6.12 Typical variation of volume fraction of fibers with the number of plies of knitted fabric.

ing n_k . However, it is to be noted that the number of layers of knitted fabrics that can be used is limited by the thickness of the composite.

Figures 6.10–6.12 give an approximate idea of variation of V_f with D_y , N and n_k . The maximum V_f that can be achieved in knitted fabric composites is yet to be estimated, as it is dependent on many other parameters such as compressibility of knitted fabrics and composite fabrication conditions. Further efforts are needed to predict the theoretical maximum V_f that can be achieved in knitted fabric composites. Experimental research works reported in the literature suggest that a fiber volume fraction of 40% is realistically possible in knitted fabric composites.

6.4.4 Micromechanical model for unidirectional fiber reinforced composite

The yarns in the crossover model shown in Fig. 6.9(b) can be divided into a number of small and straight segments. Each segment can be regarded as a transversely isotropic unidirectional composite. The conventional micromechanical models [27,28] give only four independent elastic constants (E_{11} , E_{22} , G_{12} and ν_{12}) for a transversely isotropic unidirectional composite if the constituent materials are both isotropic. We propose the following new micromechanical model that gives five independent elastic constants (E_{11} , E_{22} , G_{12} , ν_{12} , and G_{23} or ν_{23}) of the unidirectional composite [20].

Let Ox_1 be the direction parallel to the length of fiber in the sub-volume

(see Fig. 6.8). The local rectangular co-ordinate system is $Ox_1x_2x_3$, which is also called the material co-ordinate system. Let us assume that E , ν and G are the Young modulus, Poisson ratio and the shear modulus, that V represents the fraction of volume of the material, that the subscripts 'f' and 'm' stand for the fiber and the matrix respectively, and that the subscripts 1, 2 and 3 denote the material co-ordinates x_1 , x_2 and x_3 .

Let us represent the macro-stress tensors of the fiber, the matrix and the composite in a selected sub-volume by $[\sigma_{ij}^f]$, $[\sigma_{ij}^m]$ and $[\sigma_{ij}]$ respectively. Correspondingly, the macro-strain tensors are $[\epsilon_{ij}^f]$, $[\epsilon_{ij}^m]$ and $[\epsilon_{ij}]$. The two sets of tensors satisfy the following micromechanical relationships

$$[\sigma_{ij}] = V_f [\sigma_{ij}^f] + V_m [\sigma_{ij}^m] \quad [6.12]$$

$$[\epsilon_{ij}] = V_f [\epsilon_{ij}^f] + V_m [\epsilon_{ij}^m] \quad [6.13]$$

We use $[S_{ij}^f]$, $[S_{ij}^m]$ and $[S_{ij}]$ to denote the compliance matrices of the fiber, the matrix and the unidirectional composite. They have the forms

$$[S_{ij}^f] = \begin{bmatrix} \frac{1}{E_f} & -\frac{\nu_f}{E_f} & -\frac{\nu_f}{E_f} & 0 & 0 & 0 \\ -\frac{\nu_f}{E_f} & \frac{1}{E_f} & -\frac{\nu_f}{E_f} & 0 & 0 & 0 \\ -\frac{\nu_f}{E_f} & -\frac{\nu_f}{E_f} & \frac{1}{E_f} & 0 & 0 & 0 \\ 0 & 0 & 0 & \frac{1}{G_f} & 0 & 0 \\ 0 & 0 & 0 & 0 & \frac{1}{G_f} & 0 \\ 0 & 0 & 0 & 0 & 0 & \frac{1}{G_f} \end{bmatrix} = \begin{bmatrix} [S_{\sigma}^f] & [0] \\ [0] & [S_{\tau}^f] \end{bmatrix} \quad [6.14]$$

$$[S_{ij}^m] = \begin{bmatrix} \frac{1}{E_m} & -\frac{\nu_m}{E_m} & -\frac{\nu_m}{E_m} & 0 & 0 & 0 \\ -\frac{\nu_m}{E_m} & \frac{1}{E_m} & -\frac{\nu_m}{E_m} & 0 & 0 & 0 \\ -\frac{\nu_m}{E_m} & -\frac{\nu_m}{E_m} & \frac{1}{E_m} & 0 & 0 & 0 \\ 0 & 0 & 0 & \frac{1}{G_m} & 0 & 0 \\ 0 & 0 & 0 & 0 & \frac{1}{G_m} & 0 \\ 0 & 0 & 0 & 0 & 0 & \frac{1}{G_m} \end{bmatrix} = \begin{bmatrix} [S_{\sigma}^m] & [0] \\ [0] & [S_{\tau}^m] \end{bmatrix} \quad [6.15]$$

$$[S_{ij}] = \begin{bmatrix} \frac{1}{E_{11}} & -\frac{\nu_{12}}{E_{11}} & -\frac{\nu_{13}}{E_{11}} & 0 & 0 & 0 \\ -\frac{\nu_{12}}{E_{11}} & \frac{1}{E_{22}} & -\frac{\nu_{23}}{E_{22}} & 0 & 0 & 0 \\ -\frac{\nu_{13}}{E_{11}} & -\frac{\nu_{23}}{E_{22}} & \frac{1}{E_{33}} & 0 & 0 & 0 \\ 0 & 0 & 0 & \frac{1}{G_{23}} & 0 & 0 \\ 0 & 0 & 0 & 0 & \frac{1}{G_{13}} & 0 \\ 0 & 0 & 0 & 0 & 0 & \frac{1}{G_{12}} \end{bmatrix} = \begin{bmatrix} [S_{\sigma}] & [0] \\ [0] & [S_{\tau}] \end{bmatrix} \quad [6.16]$$

where $[S_{\sigma}]$ and $[S_{\tau}]$ are 3×3 sub-matrices relating normal stresses with elongation strains and shear stresses with shear strains respectively. With $[S_{ij}^f]$, $[S_{ij}^m]$ and $[S_{ij}]$, the macro-stresses and strains are connected by

$$\{\sigma_i^f\} = [S_{ij}^f] \{\epsilon_j^f\} \quad [6.17]$$

$$\{\sigma_i^m\} = [S_{ij}^m] \{\epsilon_j^m\} \quad [6.18]$$

$$\{\sigma_i\} = [S_{ij}] \{\epsilon_j\} \quad [6.19]$$

where $\{\sigma_i\} = \{\sigma_{11}, \sigma_{22}, \sigma_{33}, \sigma_{23}, \sigma_{13}, \sigma_{12}\}^T$ and $\{\epsilon_i\} = \{\epsilon_{11}, \epsilon_{22}, \epsilon_{33}, 2\epsilon_{23}, 2\epsilon_{13}, 2\epsilon_{12}\}^T$. The critical step of the present model is to find a coefficient matrix $[A_{ij}]$ such that

$$\{\sigma_i^m\} = [A_{ij}] \{\sigma_j^f\} \quad [6.20]$$

Suppose $[A_{ij}]$ has been given. Combining 6.20 and 6.12, we get

$$\{\sigma_i^f\} = (V_f[I] + V_m[A_{ij}])^{-1} \{\sigma_j\} \quad [6.21]$$

$$\{\sigma_i^m\} = [A_{ij}](V_f[I] + V_m[A_{ij}])^{-1} \{\sigma_j\} \quad [6.22]$$

where $[I]$ is a unit matrix. By virtue of 6.12, 6.13, 6.17–6.19, 6.21 and 6.22, the compliance matrix $[S_{ij}]$ of the composite is derived as

$$[S_{ij}] = (V_f[S_{ij}^f] + V_m[S_{ij}^m])[A_{ij}](V_f[I] + V_m[A_{ij}])^{-1} \quad [6.23]$$

The coefficient matrix $[A_{ij}]$ must be chosen so that the resulting compliance matrix $[S_{ij}]$ be symmetric. It is clear that $[A_{ij}]$ can be sub-divided into

$$[A_{ij}] = \begin{bmatrix} [a_{ij}] & [0] \\ [0] & [b_{ij}] \end{bmatrix}$$

where $[a_{ij}]$ and $[b_{ij}]$ are 3×3 sub-matrices such that

$$[S_{\sigma}] = (V_f [S_{\sigma}^f] + V_m [S_{\sigma}^m] [a_{ij}]) (V_f [I] + V_m [a_{ij}])^{-1} \quad [6.24]$$

$$[S_{\tau}] = (V_f [S_{\tau}^f] + V_m [S_{\tau}^m] [b_{ij}]) (V_f [I] + V_m [b_{ij}])^{-1} \quad [6.25]$$

Detailed discussions on the determinations of $[a_{ij}]$ and $[b_{ij}]$ are relatively lengthy and are out of the scope of this chapter. Here we only give a set of empirical formulae for a_{ij} and b_{ij} as below:

$$\begin{aligned} a_{11} &= E_m / E_f \\ a_{22} &= a_{33} = 0.5(1 + E_m / E_f) \\ a_{12} &= \frac{S_{12}^f - S_{12}^m}{S_{11}^f - S_{11}^m} (a_{11} - a_{22}) \end{aligned} \quad [6.26]$$

$$\begin{aligned} a_{13} &= (c_{22}d_1 - c_{12}d_2) / (c_{11}c_{22} - c_{12}c_{21}) \\ a_{23} &= (c_{11}d_2 - c_{21}d_1) / (c_{11}c_{22} - c_{12}c_{21}) \end{aligned} \quad [6.27]$$

$$b_{22} = b_{33} = 0.5(1 + G_m / G_f)$$

and all the other a_{ij} and b_{ij} but b_{11} being taken as zero. In 6.26, the parameters c_{ij} and d_i are given by

$$\begin{aligned} c_{11} &= S_{11}^m - S_{11}^f \\ c_{12} &= S_{12}^m - S_{12}^f \\ d_1 &= (a_{11} - a_{33})(S_{13}^m - S_{13}^f) \\ c_{21} &= (V_f + V_m a_{22})(S_{11}^m - S_{11}^f) \\ c_{22} &= (V_f + V_m a_{11})(S_{22}^m - S_{22}^f) + V_m (S_{12}^f - S_{12}^m) a_{12} \\ d_2 &= (V_f + V_m a_{11})(a_{22} - a_{33})(S_{23}^m - S_{23}^f) + (V_f + V_m a_{33})(S_{13}^m - S_{13}^f) a_{12} \end{aligned}$$

The expression for b_{11} is more complicated. However, we know that S_{44} is not an independent elastic constant but is determined by

$$S_{44} = \frac{1}{G_{23}} = \frac{2(1 + \nu_{23})}{E_{22}} = 2(S_{22} - S_{23}) \quad [6.28]$$

Hence, b_{11} is actually immaterial. Combining 6.24–6.28 gives the compliance matrix. The stiffness matrix is simply obtained by the inversion of the compliance matrix, i.e.

$$[C_{ij}] = [S_{ij}]^{-1} \quad [6.29]$$

6.4.5 Elastic properties in global co-ordinates

The compliance or stiffness matrix obtained above is in material co-ordinates. To obtain the overall mechanical properties of the composite, it

is necessary to transform these matrices from a local co-ordinate system to the global co-ordinate system.

Suppose that the direction cosines between the material co-ordinates Ox_1, Ox_2, Ox_3 and the global co-ordinates Ox, Oy, Oz are denoted by (l_i, m_i, n_i) where

$$l_i = \cos(x_i, x), m_i = \cos(x_i, y), n_i = \cos(x_i, z), i = 1, 2, 3 \quad [6.30]$$

By means of Equations 6.8 and 6.9, Equation 6.30 can be represented as

$$l_1 = \cos(\theta_x)\sin(\theta_z), m_1 = \sin(\theta_x)\sin(\theta_z), n_1 = \cos(\theta_z)$$

$$l_2 = -\sin(\theta_x), m_2 = \cos(\theta_x), n_2 = 0$$

$$l_3 = -\cos(\theta_x)\cos(\theta_z), m_3 = -\sin(\theta_x)\cos(\theta_z), n_3 = \sin(\theta_z)$$

With these coefficients, the two sets of co-ordinates are connected by

$$\begin{Bmatrix} x_1 \\ x_2 \\ x_3 \end{Bmatrix} = \begin{bmatrix} l_1 & m_1 & n_1 \\ l_2 & m_2 & n_2 \\ l_3 & m_3 & n_3 \end{bmatrix} \begin{Bmatrix} x \\ y \\ z \end{Bmatrix} = [e_{ij}] \begin{Bmatrix} x \\ y \\ z \end{Bmatrix} \quad [6.31]$$

We use $[\sigma_{ij}^G]$ to denote the stress tensor in the global co-ordinate system. It has the form

$$[\sigma_{ij}^G] = \begin{bmatrix} \sigma_{xx} & \sigma_{xy} & \sigma_{xz} \\ \sigma_{yx} & \sigma_{yy} & \sigma_{yz} \\ \sigma_{zx} & \sigma_{zy} & \sigma_{zz} \end{bmatrix}$$

The transformation between the global stress tensor $[\sigma_{ij}^G]$ and the local stress tensor $[\sigma_{ij}]$ obeys the rule

$$\sigma_{kl}^G = e_{ik}e_{jl}\sigma_{ij} \quad [6.32]$$

where e_{ij} are defined in (20). By using Equation 6.32, the compliance matrix of the unidirectional fiber composite (one segment of yarn in the composite) is thus transformed into the matrix in the global co-ordinate system through the following formula:

$$[\bar{S}_{ij}]_{n-1}^Y = [T_{ij}]_s^T [S_{ij}] [T_{ij}]_s \quad [6.33]$$

where the superscript Y stands for the yarn and the subscript $n - 1$ for the segment under consideration, $[T_{ij}]_s$ is a transformation matrix given by

$$[T_{ij}]_s = \begin{bmatrix} l_1^2 & l_2^2 & l_3^2 & l_2l_3 & l_3l_1 & l_1l_2 \\ m_1^2 & m_2^2 & m_3^2 & m_2m_3 & m_3m_1 & m_1m_2 \\ n_1^2 & n_2^2 & n_3^2 & n_2n_3 & n_3n_1 & n_1n_2 \\ 2m_1n_1 & 2m_2n_2 & 2m_3n_3 & m_2n_3 + m_3n_2 & n_3m_1 + n_1m_3 & m_1n_2 + m_2n_1 \\ 2n_1l_1 & 2n_2l_2 & 2n_3l_3 & l_2n_3 + l_3n_2 & n_3l_1 + n_1l_3 & l_1n_2 + l_2n_1 \\ 2l_1m_1 & 2l_2m_2 & 2l_3m_3 & l_2m_3 + l_3m_2 & l_1m_3 + l_3m_1 & l_1m_2 + l_2m_1 \end{bmatrix},$$

Similarly, by using the rule transforming the strain tensor $[\varepsilon_{ij}]$ in the local co-ordinate system to the strain tensor $[\varepsilon_{ij}^G]$ in the global co-ordinate system, we obtain the stiffness transformation formula as

$$[\overline{C}_{ij}]_{n-1}^Y = [T_{ij}]_c^T [C_{ij}] [T_{ij}]_c \quad [6.34]$$

in which the transformation matrix $[T_{ij}]_c$ is given by

$$[T_{ij}]_c = \begin{bmatrix} l_1^2 & l_2^2 & l_3^2 & 2l_2l_3 & 2l_3l_1 & 2l_1l_2 \\ m_1^2 & m_2^2 & m_3^2 & 2m_2m_3 & 2m_3m_1 & 2m_1m_2 \\ n_1^2 & n_2^2 & n_3^2 & 2n_2n_3 & 2n_3n_1 & 2n_1n_2 \\ m_1n_1 & m_2n_2 & m_3n_3 & m_2n_3 + m_3n_2 & n_3m_1 + n_1m_3 & m_1n_2 + m_2n_1 \\ n_1l_1 & n_2l_2 & n_3l_3 & l_2n_3 + l_3n_2 & n_3l_1 + n_1l_3 & l_1n_2 + l_2n_1 \\ l_1m_1 & l_2m_2 & l_3m_3 & l_2m_3 + l_3m_2 & l_1m_3 + l_3m_1 & l_1m_2 + l_2m_1 \end{bmatrix}$$

6.4.6 Assemblage in the crossover model

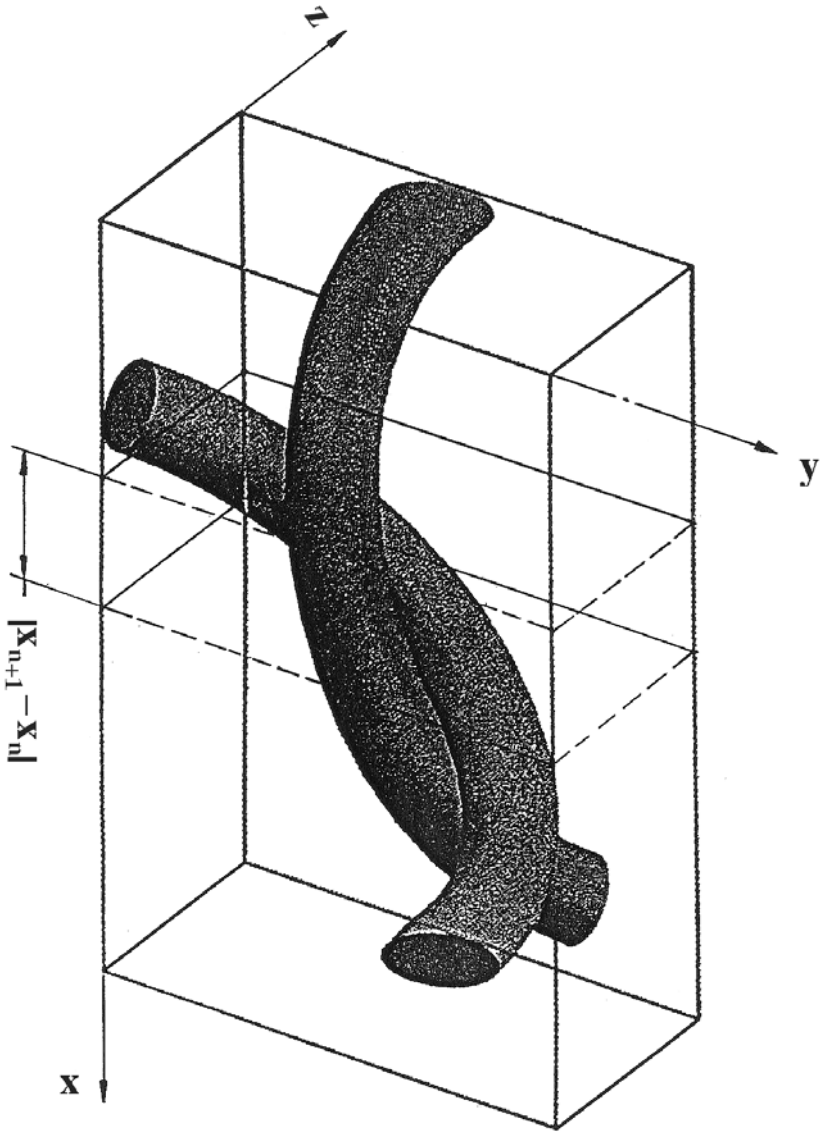
Equations 6.33 and 6.34 give the compliance and stiffness matrices of only one segment of yarn. To obtain the overall compliance and stiffness matrices of the crossover model, it is necessary to consider the contributions of all the yarn segments. The contributions of all the yarn segments are assembled using the following volume-averaging method.

To apply the volume-averaging method, the crossover model is divided into a number of sub-volumes. The material between two cross-sectional planes perpendicular to the wale direction represents one such sub-volume (Fig. 6.13). Certain sub-volumes contain one yarn segment and others contain two yarn segments. For easy analysis, each sub-volume containing two yarn segments is considered as two sub-volumes. Now each sub-volume with single yarn segment may be considered as a transversely isotropic unidirectional composite. Hence, the micromechanical formulae presented in Sections 6.4.4 and 6.4.5 can be used. In such a case, the V_f represents the overall volume fraction of fibers in the composite. The contributions of all the sub-volumes can be assembled using the following equations:

$$[\overline{S}_{ij}] = \sum_{n=1}^{M-1} \frac{|x_{n+1}^{1st} - x_n^{1st}|}{(2L)} [\overline{S}_{ij}]_n^{1st} + \sum_{n=1}^{M-1} \frac{|x_{n+1}^{2nd} - x_n^{2nd}|}{(2L)} [\overline{S}_{ij}]_n^{2nd} \quad [6.35]$$

$$[\overline{C}_{ij}] = \sum_{n=1}^{M-1} \frac{|x_{n+1}^{1st} - x_n^{1st}|}{(2L)} [\overline{C}_{ij}]_n^{1st} + \sum_{n=1}^{M-1} \frac{|x_{n+1}^{2nd} - x_n^{2nd}|}{(2L)} [\overline{C}_{ij}]_n^{2nd} \quad [6.36]$$

where $(M - 1)$ is the number of discretized yarn segments in the crossover model, the superscripts 1st and 2nd stand for the first and second yarns in the volume, and L is the projected length of one yarn on the x -axis (wale direction) of the crossover model, i.e.



6.13 Schematic representation of a typical sub-volume of the crossover model.

Table 6.2. Elastic properties of plain knitted fiber fabric composites

Fabric ($n_k t, V_f$)	Model	E_{xx} (GPa)	E_{yy} (GPa)	E_{zz} (GPa)	G_{xy} (GPa)	G_{xz} (GPa)	G_{yz} (GPa)	ν_{xy}	ν_{xz}	ν_{yz}
1 ^a	Exper.	5.38	4.37					0.48		
0.06 ^b		(0.33) ^d	(0.07)					(0.13)		
0.095 ^c	6.35	5.61	4.59	4.48	1.91	1.75	1.63	0.369	0.354	0.367
	6.36	6.59	4.90	4.66	2.20	1.89	1.67	0.382	0.353	0.375
4	Exper.	10.28	8.49							
0.07		(0.35)	(0.21)							
0.323	6.35	9.47	7.21	7.00	3.13	2.78	2.53	0.371	0.351	0.368
	6.36	13.55	8.53	7.65	4.43	3.38	2.70	0.408	0.342	0.378

The parameters used are: $E_f = 74$ GPa, $E_m = 3.6$ GPa, $\nu_f = 0.23$, $\nu_m = 0.35$, $d = 0.0445$ cm, $D_y = 1600$, $K = 0.45$, $\rho_f = 2.54$ g/cm³, $C = 2.5$ cycles/cm and $W = 2$ cycles/cm.

^a n_k (plies of the fabrics).

^b t (thickness of the composite).

^c V_f (fiber volume fraction).

^d Scatter deviation of the experiment.

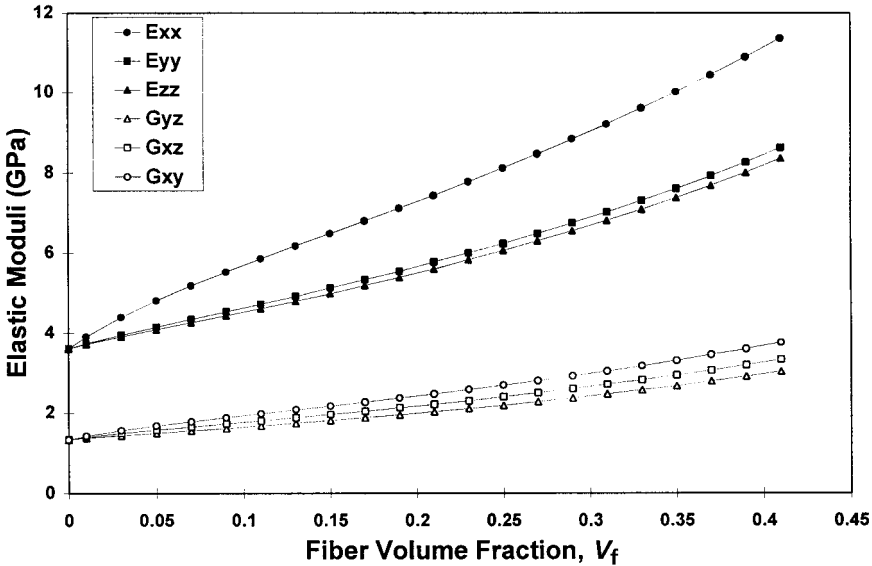
$$L = \left| x_M^{1st} - x_1^{1st} \right| = \left| x_M^{2nd} - x_1^{2nd} \right|$$

Equations 6.35 and 6.36 give the overall compliance and stiffness matrices of the crossover model respectively.

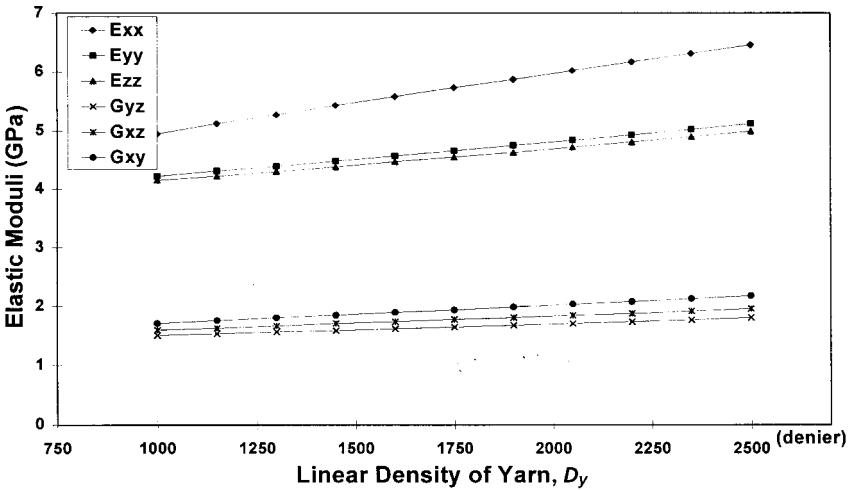
6.4.7 Elastic properties: results and discussion

To validate the analytical procedures outlined in Sections 6.4.4–6.4.6, initially predictions were made for the knitted fabric composites whose experimentally determined elastic properties were known [22,23]. Both the experimental and theoretical elastic properties of single- and four-ply knitted glass fiber fabric reinforced epoxy composites are summarized in Table 6.2. The data clearly indicate that the present analysis procedure gives a good estimate of elastic properties of knitted fabric composites. It can also be noted that Equation 6.35 gives better prediction than Equation 6.36 and, hence, the following calculations are made using Equation 6.35.

Let us investigate the role of V_f and parameters of knitted fabric on the elastic properties of the composite. Equation 6.10 suggests that V_f can be increased in three different ways: (1) by increasing the linear density of the yarn (D_y); (2) by increasing stitch density of knitted fabric (N); and (3) by increasing number of plies of knitted fabric (n_k). The elastic constants versus various of these parameters are thus calculated and are shown in Figs. 6.14–6.17. Only the Young moduli and the shear moduli are reported since the Poisson ratio has shown little dependence on the V_f or knitted fabric

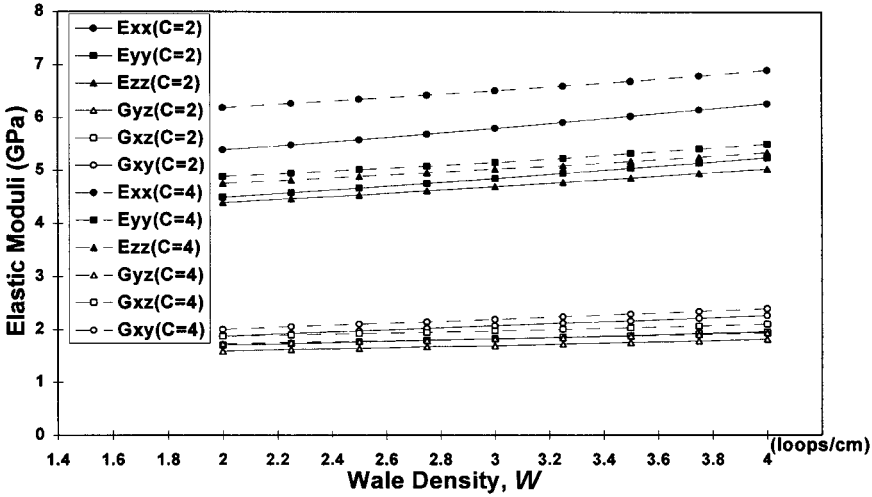


6.14 Typical variation of elastic moduli of knitted glass fiber fabric reinforced epoxy composite with the fiber volume fraction.

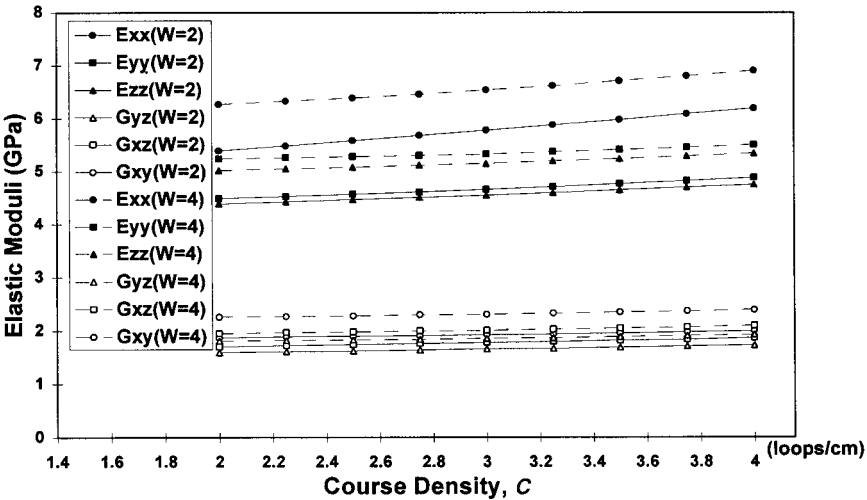


6.15 Typical variation of elastic moduli of knitted glass fiber fabric reinforced epoxy composite with the linear density of yarn.

parameters as long as V_f is not large. The results clearly indicate that the elastic moduli are dependent almost linearly on either of the parameters, yarn linear density (denier), wale density (W) or course density (C), but slightly non-linearly on the V_f .



6.16 Typical variation of elastic moduli of knitted glass fiber fabric reinforced epoxy composite with the course density of the fabric.



6.17 Typical variation of elastic moduli of knitted glass fiber fabric reinforced epoxy composite with the wale density of the fabric.

6.5 Analysis of tensile strength properties

6.5.1 Prediction of tensile strength

As described in Section 6.3, the failure strength of knitted fabric reinforced epoxy composites mainly depends on the yarn bundles bridging the frac-

Copyrighted Material downloaded from Woodhead Publishing Online
 Delivered by http://woodhead.metapress.com
 Hong Kong Polytechnic University (714-57-975)
 Saturday, January 22, 2011 12:30:57 AM
 IP Address: 158.132.122.9

ture plane (Fig. 6.6). The number of yarns bridging the fracture plane would depend on the testing direction with respect to the knitted fabric. The number of yarn bundles bridging the wale $[n_w]_b$ and course $[n_c]_b$ fracture planes are given by

$$[n_w]_b = n_k(2) \frac{W}{2} B \quad [6.37]$$

$$[n_c]_b = n_k \frac{C}{2} B$$

where B is the width of tensile specimen in cm.

The area fractions of yarn bundles bridging the wale $[A_w]_b$ and course $[A_c]_b$ fracture plane are given by

$$[A_w]_b = \frac{n_k W \pi d^2}{4t}$$

$$[A_c]_b = \frac{n_k C \pi d^2}{8t} \quad [6.38]$$

where t is the specimen thickness in cm, d is the yarn diameter given by Equation 6.7. The knitted fabric composite strengths in the wale (σ_w) and course (σ_c) directions are given by

$$\sigma_w = \frac{n_k W \pi d^2 [\bar{\sigma}_b]}{4t}$$

$$\sigma_c = \frac{n_k C \pi d^2 [\bar{\sigma}_b]}{8t} \quad [6.39]$$

where $\bar{\sigma}_b$ is the mean strength of set of yarn bundles bridging the fracture plane. The $\bar{\sigma}_b$ can be estimated using the following procedure.

Assuming that all the bridging yarns possess the same tensile strength and are aligned perfectly in the loading direction, the $\bar{\sigma}_b$ will be equal to the longitudinal tensile strength of unidirectional lamina (σ_1):

$$\bar{\sigma}_b = \sigma_1 = (\sigma_f)(V_{yf}) + (\sigma_m)(1 - V_{yf}) \quad [6.40]$$

where σ_f and σ_m are the tensile strengths of reinforcement fibers and matrix resin, respectively. V_{yf} is the volume fraction of fibers in the yarn bundle.

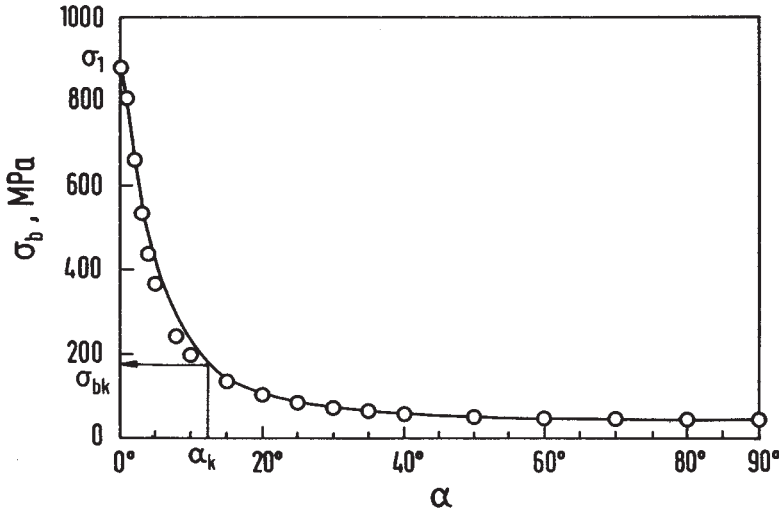
However, owing to their looped architecture, it is reasonable to assume that the yarns in the fracture plane orient at an angle α with respect to the loading direction. For tensile testing in wale direction, an approximate estimate of α can be obtained using Equations 6.8 and 6.9:

$$\cos \alpha = (\cos \theta_x)(\cos \theta_z)$$

The yarn bundle can be treated as off-axis loaded unidirectional lamina. Hence, the tensile strength of a yarn bundle is given by [28]:

Table 6.3. Tensile properties of unidirectional glass fiber/epoxy lamina

Fiber volume fraction (V_{vf})	Longitudinal strength, σ_1 (MPa)	Transverse strength, σ_2 (MPa)	Shear strength, τ_{12} (MPa)
0.45	885	45	35

6.18 Typical variation of σ_b with α .

$$\sigma_b = \left[\frac{\cos^4 \alpha}{\sigma_1^2} + \frac{\sin^4 \alpha}{\sigma_2^2} + \frac{\sin^2 \alpha \cos^2 \alpha}{\tau_{12}^2} - \frac{\sin^2 \alpha \cos^2 \alpha}{\sigma_1^2} \right]^{\frac{1}{2}} \quad [6.41]$$

where σ_1 , σ_2 and τ_{12} are respectively the longitudinal, transverse and shear strengths of unidirectional lamina given in Table 6.3.

Typical variation of σ_b with α is shown in Fig. 6.18. σ_b decreased with increasing α . The decrease of σ_b was significant in the range $0^\circ < \alpha < 15^\circ$. Hence, the variation of σ_b with α in this range on the composite strength is analyzed. All the yarn bundles in the fracture plane may not have the same α value, since the fracture path is irregular and occurs at different positions of the knit loops. During tensile testing the yarn bundles are peeled (debonded) from the fracture surface and stretched before their failure. Owing to the peeling and stretching effect, the yarn bundles try to align in the testing direction. Determination of actual α just before the failure of yarn bundle is a difficult task. It may be the case that different yarn bundles

orient at different α with respect to the loading direction. Because of different values of α , it can be expected that yarn bundles bridging the fracture plane possess different strength values. The yarn bundles may possess different strengths due to the statistical nature of fiber strength. Many researchers investigated the statistical nature of bundle strengths. The present study is mainly concerned with the variation of σ_b with α . From Fig. 6.18, an exponential relationship between σ_b and α is given by

$$\sigma_b = Pe^{-Q\alpha} \quad [6.42]$$

where P and Q are parameters of exponential function and can be determined using Equations 6.43 and 6.44, respectively.

When $\alpha = 0$,

$$P = \sigma_1 \quad [6.43]$$

Assume that all the yarn bundles are oriented in the range $0 < \alpha < \alpha_k$. The maximum orientation, α_k , can be determined from the fracture surfaces. σ_{bk} is the bundle strength corresponding to the maximum orientation α_k . From Equations 6.42 and 6.43,

$$\sigma_{bk} = \sigma_1 e^{-Q\alpha_k}$$

Rearranging gives

$$Q = \frac{1}{\alpha_k} \ln\left(\frac{\sigma_1}{\sigma_{bk}}\right) \quad [6.44]$$

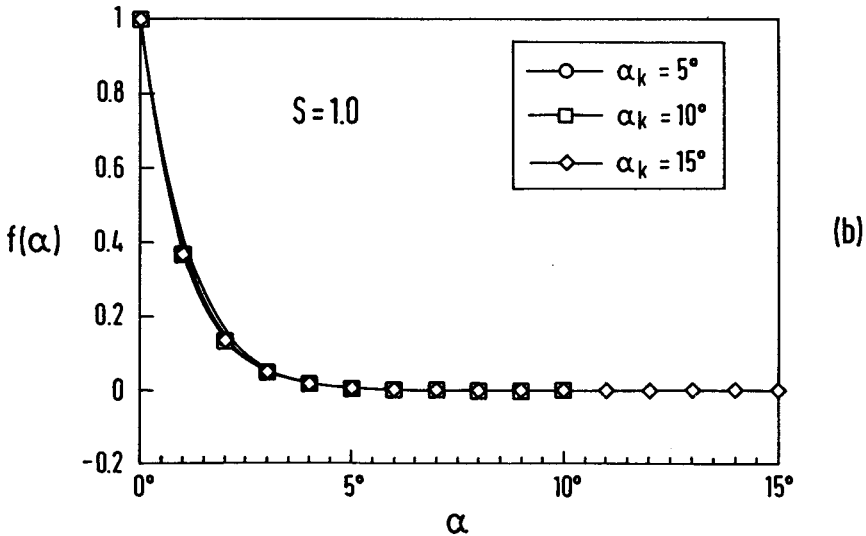
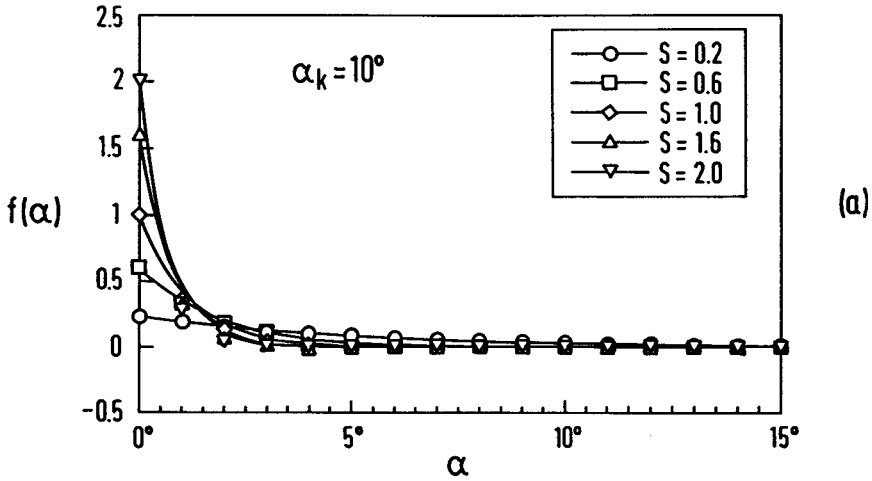
Equation 6.42 indicates the changes in σ_b with α . Equation 6.37 gives the number of yarn bundles bridging the fracture plane. It is necessary to know how many of these bundles orient at each value of α . The following exponential function $f(\alpha)$ was assumed for expressing the orientation distribution of yarn bundles in the fracture plane:

$$f(\alpha) = Re^{-S\alpha} \quad [6.45]$$

where R and S are the parameters of the exponential function. This function suggests that more yarns orient close to the testing direction. This assumption is reasonable as the yarn bundles try to align in the loading direction due to the debonding and stretching mechanisms. Typical curves for the function $f(\alpha)$ are shown in Fig. 6.19. The area under a curve is unity, therefore

$$\int_0^{\alpha_k} f(\alpha) d\alpha = \int_0^{\alpha_k} Re^{-S\alpha} d\alpha = -\frac{R}{S}(e^{-S\alpha_k} - 1) = 1$$

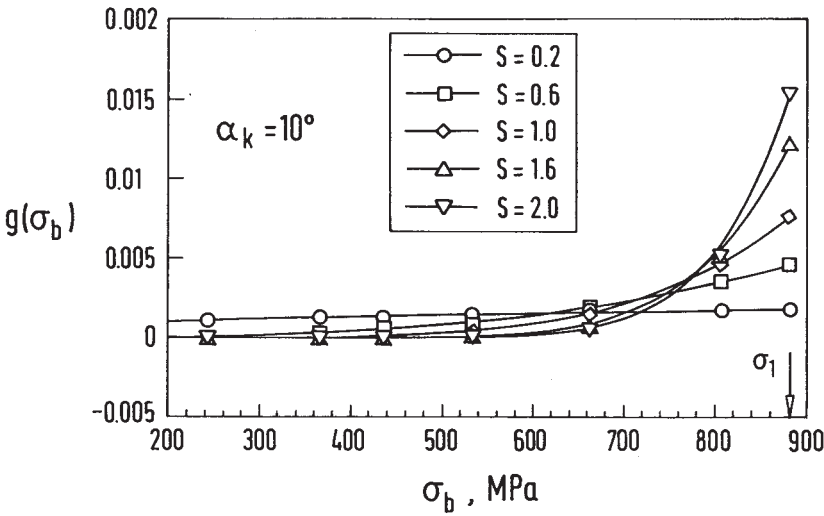
$$R = \frac{S}{(1 - e^{-S\alpha_k})} \quad [6.46]$$



6.19 Typical curves of function $f(\alpha)$.

R is dependent on the values of S and α_k . Typical $f(\alpha)$ curves for different S and α_k are shown in Fig. 6.19. These curves indicate that $f(\alpha)$ is more sensitive to the parameter S than α_k . When S is small, the yarn orientation distribution is spread out. For large values of S , the distribution is skewed and more yarns are aligned close to the loading direction.

Let $g(\sigma_b)$ be the function of yarn bundle distribution with respect to the



6.20 Typical curves of function $g(\sigma_b)$.

bundle strength. Typical $g(\sigma_b)$ curves are shown in Fig. 6.20. Using the variable transformation technique,

$$g(\sigma_b)d\sigma_b = f(\alpha)d\alpha$$

Rearranging gives

$$g(\sigma_b) = f(\alpha) \left| \frac{d\alpha}{d\sigma_b} \right| \tag{6.47}$$

From Equations 6.42 and 6.47,

$$g(\sigma_b) = \frac{R}{PQ} e^{(Q-S)\alpha} \tag{6.48}$$

From Equation 6.42,

$$\alpha = -\frac{1}{Q} \ln\left(\frac{\sigma_b}{P}\right) \tag{6.49}$$

Combining Equations 6.48 and 6.49,

$$g(\sigma_b) = \frac{R}{QP^{S/Q}} \sigma^{(S/Q-1)} \tag{6.50}$$

Let $G(\sigma_b)$ indicate the yarn bundles fractured due to the applied stress, σ_b . The surviving yarn bundles $[1 - G(\sigma_b)]$ are given by

$$[1 - G(\sigma_b)] = \int_{\sigma_b}^{\sigma_1} g(\sigma_b)d\sigma_b$$

or

$$[1 - G(\sigma_b)] = \frac{R}{SP^{S/Q}} [\sigma_1^{S/Q} - \sigma_b^{S/Q}] \quad [6.51]$$

Let σ_{bm} be the value of bundle stress σ_b which gives $\sigma_b[1 - G(\sigma_b)]$ its maximum value, namely

$$\frac{d}{d\sigma_b} \{\sigma_b [1 - G(\sigma_b)]\}_{\sigma_b = \sigma_{bm}} = 0 \quad [6.52]$$

Equation 6.52 implies that the maximum yarn bundle stress, σ_{bm} , is found from the condition that at failure the load borne by the bundles is the maximum. Hence,

$$\sigma_{bm} = P \left[\frac{1}{1 + (S/Q)} \right]^{-Q/S} \quad [6.53]$$

The maximum mean strength ($\bar{\sigma}_b$) of surviving yarn bundles can be obtained by substituting the value of σ_{bm} in $\sigma_b[1 - G(\sigma_b)]$:

$$\bar{\sigma}_b = \frac{RP}{Q} \left[\frac{1}{1 + (S/Q)} \right]^{Q/S+1} \quad [6.54]$$

For a given composite system, the parameter P is constant (Equation 6.43). Q is mainly dependent on the α_k and σ_{bk} (Equation 6.44). Parameter R is dependent on S and α_k (Equation 6.46). In other words, $\bar{\sigma}_b$ mainly depends on S and α_k . Typical variation of $\bar{\sigma}_b$ with S and α_k is shown in Fig. 6.21, which clearly indicates that $\bar{\sigma}_b$ is mainly influenced by the parameter S . The $\bar{\sigma}_b$ initially increased rapidly with increasing S from 0.2 to 2.5, above which it increased only marginally. This behavior is expected since large S means a greater number of yarns aligned close to the loading direction and hence higher mean bundle strength. Small values of S indicate that yarn orientation distribution is spread out and, hence, mean bundle strength is lower.

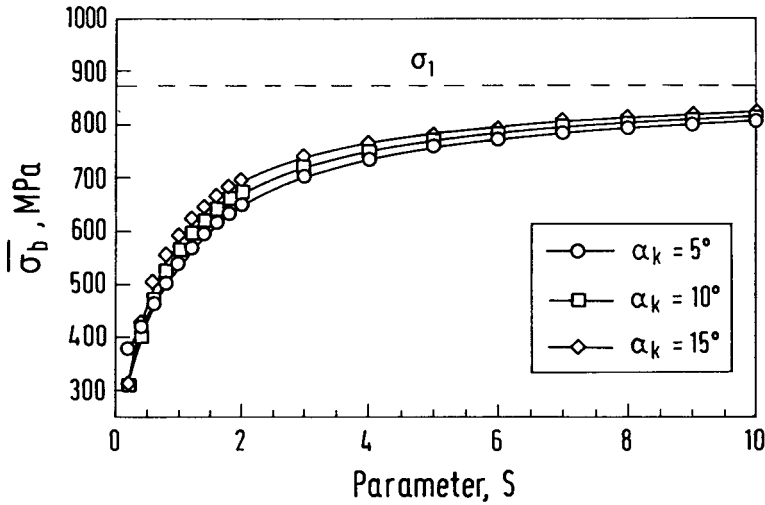
Substituting Equation 6.54 in Equation 6.39, the knitted fabric composite tensile strengths in the wale (σ_w) and course (σ_c) directions are given by

$$\sigma_w = \left(\frac{n_k W \pi d^2}{4t} \right) \left\{ \frac{RP}{Q} \left[\frac{1}{1 + S/Q} \right]^{Q/S+1} \right\} \quad [6.55]$$

$$\sigma_c = \left(\frac{n_k C \pi d^2}{8t} \right) \left\{ \frac{RP}{Q} \left[\frac{1}{1 + S/Q} \right]^{Q/S+1} \right\} \quad [6.56]$$

6.5.2 Tensile strength: results and discussion

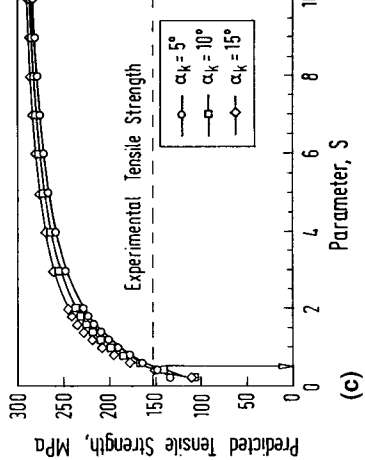
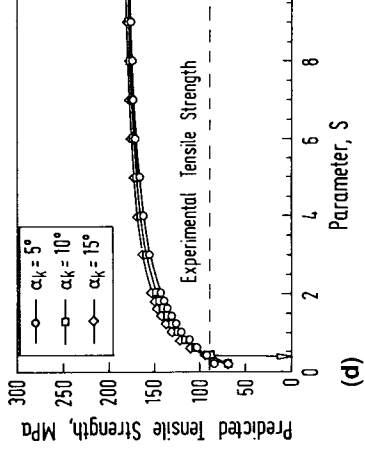
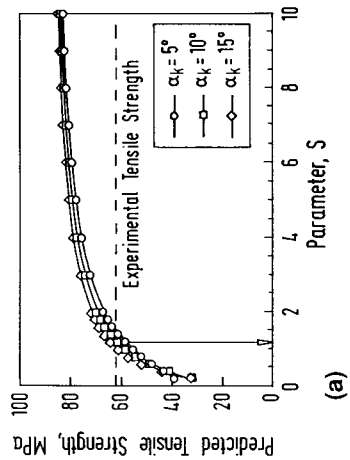
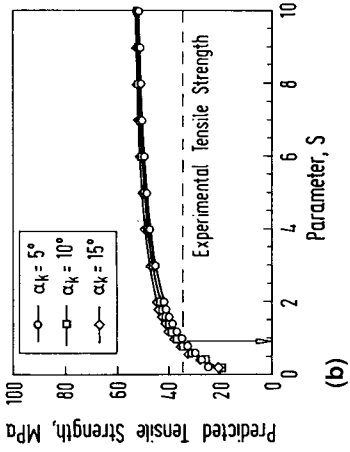
Tensile strengths of knitted fabric composites with different V_f are computed using Equation 6.55. The main assumptions are: (1) in the fiber



6.21 Typical variation of $\bar{\sigma}_b$ with parameters S and α_k .

content range investigated, the failure mechanisms of knitted fabric composites are similar and (2) the composite strength is determined mainly by the fracture strength of the yarns bridging the fracture plane. Again let us consider single- and four-ply knitted fabric composites with $V_f = 0.0933$ and 0.3198 , respectively, described in Section 6.4.3. Figure 6.22 shows the variation of predicted tensile strength with the parameters S and α_k . The composite strength is more sensitive to the parameter S than α_k . This behavior is similar to the variation of mean bundle strength, $\bar{\sigma}_b$ with S and α_k (Fig. 6.21). The predicted strength increased rapidly with increasing S from 0.2 to 2, above which it increased marginally. Larger S means that more yarns aligned close to the loading direction and hence higher tensile strength. Smaller S indicates that yarn orientation distribution is spread out and hence lower tensile strength. Table 6.4 summarizes composite strengths for different S in the range from 0.2 to 10.0. For $S = 0.2$ and $S = 10.0$, the predicted values indicate lower and upper bounds of tensile strength of knitted fabric composites. The limit of lower bound would depend on the parameter S . It is necessary to determine S precisely for accurate estimation of composite tensile strength. For this purpose, the experimental tensile strengths are shown as dashed lines in Fig. 6.22. From Fig. 6.22, the critical value of parameter S corresponding to which predicted strength matches with the experimental result can be identified. In the case of single-ply composite, both the wale and course predicted tensile strengths match approximately with the respective experimental results when $S = 1.0$. In the case of four-ply composite, when $S = 0.5$ the wale and course predicted

Copyrighted Material downloaded from Woodhead Publishing Online
 Delivered by http://woodhead.metapress.com
 Hong Kong Polytechnic University (714-57-975)
 Saturday, January 22, 2011 12:30:57 AM
 IP Address: 158.132.122.9



6.22 Variation of predicted tensile strength of knitted fabric composite with parameters S and α_k : (a) wale specimen with $V_f = 0.0933$; (b) course specimen with $V_f = 0.0933$; (c) wale specimen with $V_f = 0.3198$; and (d) course specimen with $V_f = 0.3198$.

Table 6.4. Tensile properties of plain knitted glass fiber fabric/epoxy composite

Number of plies of knitted fabric, n_k	Testing direction	Experimental tensile strength (MPa)	Analytical tensile strength (MPa)		
			$S = 0.2$	$S = 1.0$	$S = 10.0$
1	Wale	62.83 (7.1)	31.83	60.0	84.75
4	Wale	152.7 (9.5)	109.1	150.0	290.6
1	Course	35.5 (2.21)	19.85	36.0	52.96
4	Course	75.4 (4.5)	68.2	85.0	181.6

strengths match approximately with the respective experimental strengths. In other words, it appears that the critical S is dependent on the number of plies of knitted fabric used for reinforcing the composite material. This may be due to the mismatch between the adjacent plies of knitted fabrics. Further detailed experiments are necessary to establish clearly the dependence of critical value of the parameter S on the variables such as number of plies of knitted fabric, fabric stitch density and linear density of yarn. This will enable accurate prediction of tensile strengths of knitted fabric composites with different fiber volume fractions.

In the present study, only the variation of orientation of bridging yarns is considered. The fracture process of a set of bridging yarns would depend on the yarn orientation distribution as well as the yarn strength distribution. The preliminary procedure outlined here may be further modified by considering the statistical nature of yarn strengths for accurate determination of composite strength.

Both the experimental and predicted results (Tables 6.3 and 6.4) suggest that the plain weft knitted fabric composites possess superior tensile properties in the wale direction compared with the course direction. This is mainly due to the higher proportion of yarns oriented in the wale direction than in the course direction. Tensile properties increase with increasing fiber content.

6.6 Conclusions

Preliminary methodologies for predicting the tensile properties of plain knitted fabric reinforced composites are established. Elastic properties were predicted using the crossover model and volume-averaging method. Tensile strength properties were predicted by estimating the fracture strength of yarns bridging the fracture plane. The predicted tensile properties compare favorably with the experimental results. A more detailed

analysis is necessary to assess fully the applicability and limitations of these analysis methods.

Tensile properties of knitted fabric composites can be increased with increasing fiber content. It has been shown that the fiber content of the composite can be increased by increasing (a) the linear density of yarn, (b) the stitch density of knitted fabric and (c) the number of plies of knitted fabric.

6.7 References

1. Ramakrishna, S., Hamada, H., Kotaki, M., Wu, W.L., Inoda, M. and Maekawa, Z., 'Future of knitted fabric reinforced polymer composites', in *Proc. of 3rd Japan International SAMPE Symposium*, Tokyo, 1993, pp. 312–317.
2. Horsting, K., Wulhorst, B., Franzke, G. and Offermann, P., 'New types of textile fabrics for fiber composites'. *SAMPE J.*, **29**, 7–12, 1993.
3. Dewalt, P.L. and Reichard, R.P., 'Just how good are knitted fabrics?', *J. Reinf. Plast. Comp.*, **13**, 908–917, 1994.
4. Mayer, J., Ruffieux, K., Tognini, R. and Wintermantel, E., 'Knitted carbon fibers, a sophisticated textile reinforcement that offers new perspectives in thermo-plastic composite processing', in *Proc. of ECCM6*, Bordeaux, 1993, pp. 219–224.
5. Ramakrishna, S., Hamada, H., Rydin, R. and Chou, T.W., 'Impact damage resistance of knitted glass fiber fabric reinforced polypropylene composite laminates', *Sci. Eng. Comp. Mater.*, **4**(2), 61–72, 1995.
6. Ramakrishna, S. and Hull, D., 'Energy absorption capability of epoxy composite tubes with knitted carbon fiber fabric reinforcement', *Comp. Sci. Technol.*, **49**, 349–356, 1993.
7. Ramakrishna, S., 'Energy absorption behaviors of knitted fabric reinforced epoxy composite tubes', *J. Reinf. Plast. Comp.*, **14**, 1121–1141, 1995.
8. Ramakrishna, S., Hamada, H. and Hull, D., 'The effect of knitted fabric structure on the crushing behavior of knitted glass/epoxy composite tubes', in *Impact and Dynamic Fracture of Polymers and Composites* (ESIS19), Williams, J.G. and Pavan, A., eds, Mechanical Engineering Publications, London, 1995, pp. 453–464.
9. Rudd, C.D., Owen, M.J. and Middleton, V., 'Mechanical properties of weft knit glass fiber/polyester laminates', *Comp. Sci. Technol.*, **39**, 261–277, 1990.
10. Gommers, B., Verpoest, I. and Houtte, P.V., 'Modelling the elastic properties of knitted fabric reinforced composites', *Comp. Sci. Technol.*, **56**, 685–694, 1996.
11. Ramakrishna, S., 'Characterization and modeling of tensile properties of plain knitted fabric reinforced composites', *Comp. Sci. Technol.*, **57**, 1–22, 1997.
12. Ko, F.K., Pastore, C.M., Yang, J.M. and Chou, T.W., 'Structure and properties of multilayer multidirectional warp knit fabric reinforced composites', in *Proc. of 3rd Japan-US Conference*, Tokyo, 1986, pp. 21–28.
13. Ramakrishna, S., Hamada, H., Kanamaru, R. and Maekawa, Z., 'Mechanical properties of 2.5 dimensional warp knitted fabric reinforced composites', in *Design and Manufacture of Composites*, Hoa, S.V., ed., Corcordia University, Montreal, 1994, pp. 254–263.
14. Ramakrishna, S. and Hull, D., 'Tensile behavior of knitted carbon-fiber-fabric/epoxy laminates – part I: experimental', *Comp. Sci. Technol.*, **50**, 237–247, 1994.

15. Ramakrishna, S. and Hull, D., 'Tensile behavior of knitted carbon-fiber-fabric/epoxy laminates – part II: prediction of tensile properties', *Comp. Sci. Technol.*, **50**, 249–258, 1994.
16. Ramakrishna, S., 'Analysis and modeling of plain knitted fabric reinforced composites', *J. Composite Mater.*, **31**, 52–70, 1997.
17. Ramakrishna, S., Hamada, H. and Cheng, K.B., 'Analytical procedure for the prediction of elastic properties of plain knitted fabric reinforced composites', *Composites Part A*, **28A**, 25–37, 1997.
18. Tay, T.E., Ramakrishna, S. and Jin, W., 'Three dimensional modeling of damage in plain weft knitted fabric composites', *Composites Sci. Technol.* (in press).
19. Ramakrishna, S., 'Analytical and finite element modeling of elastic behavior of plain-weft knitted fabric reinforced composites', *Key Eng. Mater.*, **137**, 71–78, 1998.
20. Ramakrishna, S. and Huang, Z.M., 'A micromechanical model for mechanical properties of two constituent composite materials', *Adv. Composite Lett.*, **6**, 43–46, 1997.
21. Ramakrishna, S., Huang, Z.M., Teoh, S.H., Tay, A.O.O. and Chew, C.L., 'Application of Leaf and Glaskin's model for estimating the 3D elastic properties of knitted fabric composites', *J. Textile Inst.* (in press).
22. Ramakrishna, S., Fujita, A., Cuong, N.K. and Hamada, H., 'Tensile failure mechanisms of knitted glass fiber fabric reinforced epoxy composites', in *Proc. of 4th Japan International SAMPE Symposium & Exhibition*, Tokyo, 1995, pp. 661–666.
23. Ramakrishna, S., Cuong, N.K., Fujita, A. and Hamada, H., 'Tensile properties of plain weft knitted glass fiber fabric reinforced epoxy composites', *J. Reinf. Plast. Comp.*, **16**, 946–966, 1997.
24. Ramakrishna, S., Hamada, H. and Cuong, N.K., 'Fabrication of knitted glass fiber fabric reinforced thermoplastic composite laminates', *J. Adv. Comp. Lett.*, **3**(6), 189–192, 1994.
25. Ramakrishna, S., Hamada, H., Cuong, N.K. and Maekawa, Z., 'Mechanical properties of knitted fabric reinforced thermoplastic composites', in *Proc. of ICCM-10*, Vancouver, August, 1995, Vol. IV, pp. 245–252.
26. Ramakrishna, S., Tang, Z.G. and Teoh, S.H., 'Development of a flexible composite material', *Adv. Composite Lett.*, **6**(1), 5–8, 1997.
27. Chamis, C.C., 'Mechanics of composite materials: past, present, and future', *J. Comp. Technol. Res.*, **11**, 3–14, 1989.
28. Tsai, S.W. and Hahn, H.T., *Introduction to Composite Materials*, Technomic Publishing, Pennsylvania, PA 1980, chapter 9.